

Density-compensated overturning in the Labrador Sea

Sijia Zou 1,4*, M. Susan Lozier¹, Feili Li^{1,5}, Ryan Abernathey² and Laura Jackson ³

The Atlantic Meridional Overturning Circulation, a key constituent of the climate system, is projected to slow down in the twenty-first century due to a weakening of the Labrador Sea convection, itself a response to greenhouse gas warming and/or enhanced freshwater flux from the Arctic. However, the first observations from the Overturning in the Subpolar North Atlantic Program reveal a minimal response of the Meridional Overturning Circulation to the strong Labrador Sea convection during the winters of 2015–2016. From an analysis of the observational and reanalysis data, we show here that this weak response can be explained by a strong density compensation in the Labrador Sea. Although convection induces important changes of temperature and salinity in the basin interior, the export of the thermal and haline anomalies to the boundary current largely takes place along density surfaces. As a result, the transformation across density surfaces, that is, the imprint on the overturning circulation, is relatively small. This finding highlights the critical relationship between temperature and salinity in determining the overturning strength in the Labrador Sea and underlines the necessity of accurate freshwater flux estimates for improved Meridional Overturning Circulation predictions.

alaeo-oceanographic and modelling studies consistently link the meridional overturning circulation (MOC) variability to the strength of Labrador Sea convection¹⁻³. However, assessing the importance of convection to the MOC has been stymied by the relatively large uncertainty of the indirect estimates of the diapycnal (that is, across density surfaces) mass flux in the Labrador Sea (2–10 Sv; 1 Sv = 10⁶ m³ s⁻¹) (Supplementary Information)⁴⁻⁹.

Recent observational studies provided new insights into the linkage between Labrador Sea convection and the MOC. The Overturning in the Subpolar North Atlantic Program (OSNAP) provided continuous measurements for the MOC in density space across the Labrador Sea from August 2014 to April 2016^{10,11}. With a mean of 3.3 Sv and a monthly s.d. of 1.1 Sv, the weak Labrador Sea MOC contributes minimally to the total overturning circulation in the subpolar North Atlantic (14.9 Sv; Fig. 1a). This finding is especially surprising because convection in the Labrador Sea during the 2015-2016 winters, among the largest ever observed¹², was expected to significantly strengthen the MOC. A similarly small MOC in the Labrador Sea (2 Sv) was reported based on a composite of hydrographic sections during 1990-1997, years over which the basin experienced strong wintertime convection⁵. That study further showed that heat transport across the Labrador Sea was accomplished primarily along density surfaces (that is, by means of the horizontal gyre circulation) with little contribution from the MOC, a partitioning attributed to a large degree of density compensation by temperature and salinity. This work, and the recent OSNAP observations, raise the question as to how density compensation impacts the MOC strength and whether the compensated relationship is persistent with time.

To answer these questions, we used the 21-month continuous observations from OSNAP to analyse the transport and water mass structure along OSNAP West (from the Labrador shelf to the southwestern tip of Greenland; Fig. 1b inset), and then compared the transformation in density space with that in temperature (θ)

and salinity (*S*) space. The analysis is repeated for a longer temporal record using an ocean reanalysis dataset.

Transport and water mass structure along OSNAP West

The Labrador Sea is characterized by strong boundary currents and weak flow in the basin interior^{13,14} (Fig. 1b). Waters enter the basin via the West Greenland Current (WGC) and exit in the Labrador Current (LC). The two boundary currents have similar vertical transport structures, but they carry waters of distinct properties (Fig. 2). Above the shelf break, cold and fresh waters ($\theta < 2.0$ °C, S < 34.10) from the Nordic Seas are transported into the basin by the WGC. On the other side of the basin, the LC exports the coldest fresh waters (θ <0.2 °C, S<34.00). These waters primarily originate from Baffin Bay and Hudson Bay. Seaward of the shelf and below the surface layer (~200-1,000 m), the WGC carries warmer and saltier Atlantic-origin waters ($\theta \approx 4.5$ °C, $S \approx 34.94$) into the Labrador Sea. As these waters are advected downstream, the instability of the WGC facilitates property exchange with the large reservoir of cold and fresh Labrador Sea Water (LSW), the product of convection, in the basin interior^{15,16} (Fig. 2). Additionally, direct heat loss and freshwater input within the boundary current may also lead to property modification of these waters. As a result, the exiting LC is much colder and fresher compared to the incoming WGC at these intermediate depths.

In the deep layer (below ~1,500 m), the overflow waters, which include the relatively salty Northeast Atlantic Deep Water (NEADW; $\theta \approx 2.8$ °C, $S \approx 34.92$) and the fresh Denmark Strait Overflow Water (DSOW; $\theta \approx 1.5$ °C, $S \approx 34.90$), flow into the basin via the WGC. The properties of these deep waters in the LC are similar to those in the WGC, with slight modifications. The 21-month mean (August 2014 to April 2016) transport of the entire WGC is 41.5 Sv, with a monthly s.d. of 4.4 Sv. This number roughly equals the total transport of all the waters that exit the basin (-43.1 ± 4.4 Sv), with the difference of -1.6 Sv due to the Arctic throughflow from the Davis Strait¹⁷.

Duke University, Durham, NC, USA. 2Columbia University/Lamont Doherty Earth Observatory, New York, NY, USA. 3Met Office, Exeter, UK.

⁴Present address: Woods Hole Oceanographic Institution, Woods Hole, MA, USA. ⁵Present address: Georgia Institute of Technology, Atlanta, GA, USA.

^{*}e-mail: szou@whoi.edu

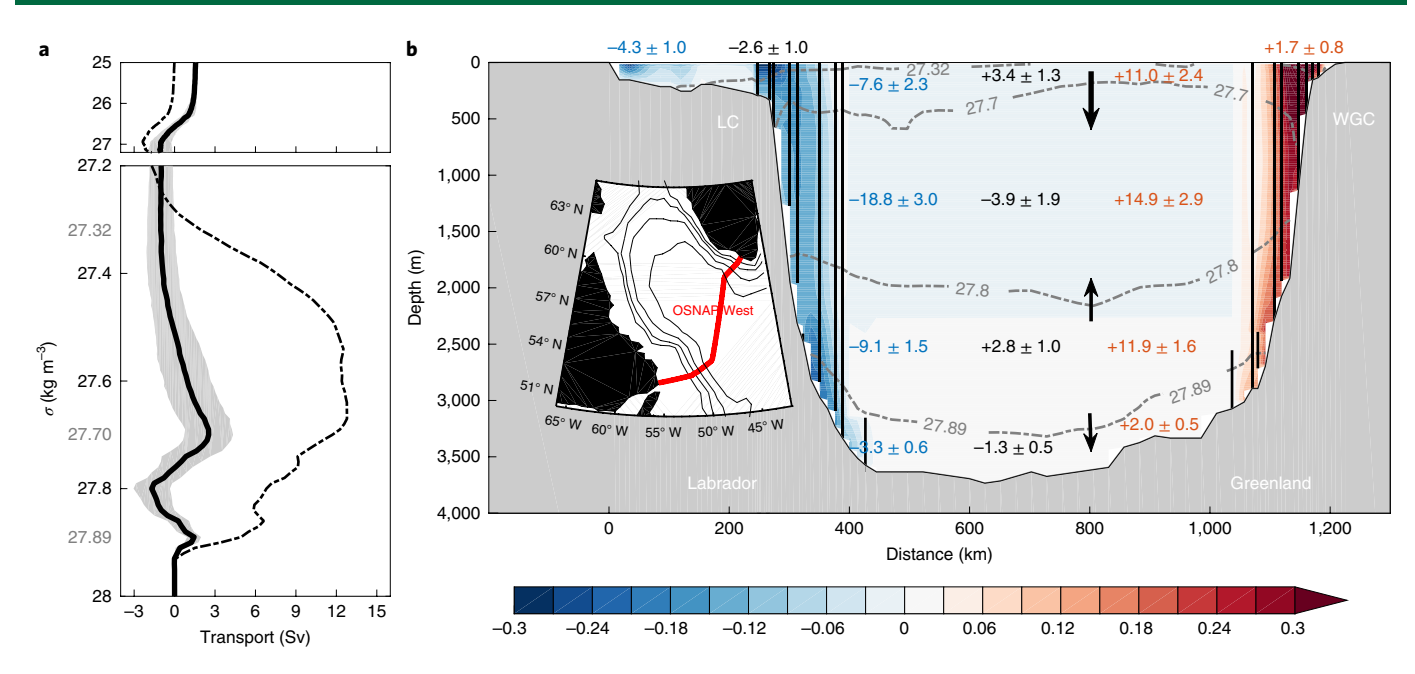


Fig. 1 Observed circulation along OSNAP West. **a**, The mean overturning streamfunction from August 2014 to April 2016 along OSNAP West (solid black), with its monthly s.d. shaded in grey. The mean overturning streamfunction along the entire OSNAP line (from Labrador to Scotland) is plotted in dashed black. **b**, The mean velocity perpendicular to OSNAP West (unit: m s⁻¹). The OSNAP West section is shown in the inset. Positive (negative) velocities indicate flow into (out of) the basin. Black lines show mooring locations and dashed grey contours denote density surfaces. The transport (mean ± monthly s.d., unit: Sv) of the total inflow (outflow) in each density class is labelled in red (blue), with the net transport labelled in black. Arrows indicate the directions of diapycnal transformation.

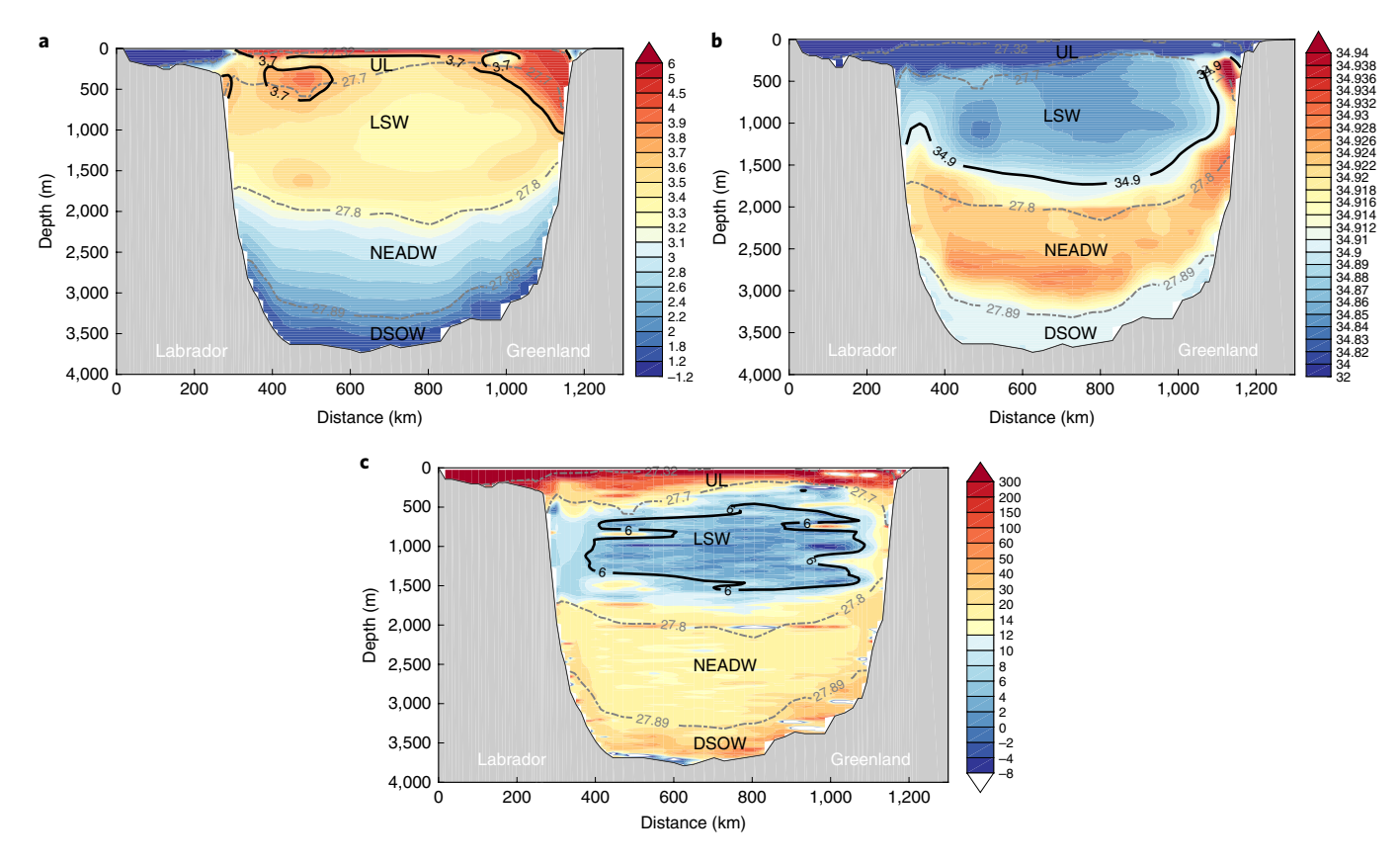


Fig. 2 | **Observed property fields along OSNAP West. a**, The 21-month mean potential temperature (°C). The black contour shows the 3.7 °C isotherm, at which the maximum overturning in temperature space is reached (Fig. 3b). **b**, The 21-month mean salinity. Here, the isohaline of 34.90 (at which the maximum overturning in salinity space is reached; Fig. 3c) is contoured in black. **c**, The 21-month mean potential vorticity (10^{-12} m⁻¹s⁻¹). The contoured isopleth of 6×10^{-12} m⁻¹s⁻¹ denotes the newly formed LSW. Potential densities are plotted in dashed grey. UL, upper layer; LSW, Labrador Sea Water; NEADW, Northeast Atlantic Deep Water; DSOW, Denmark Strait Overflow Water.

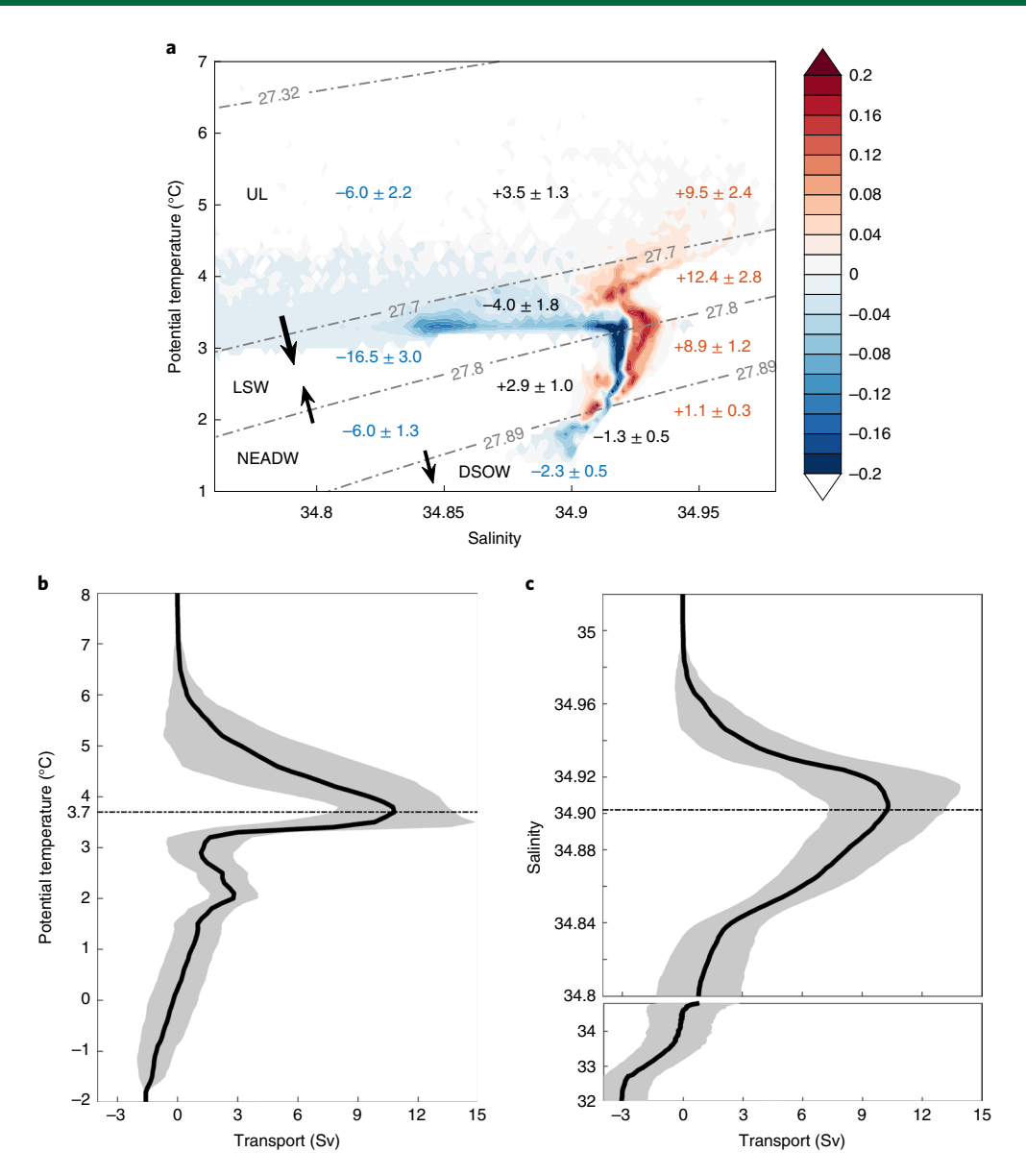


Fig. 3 | Observed transformation in θ -**S** space. **a**, The 21-month mean volume flux in θ -S space (unit: Sv). Positive (negative) transport in each grid box ($\Delta\theta$ = 0.1 °C, Δ S = 0.002) indicates that waters with the same temperature and salinity flow into (out of) the basin. The total positive (negative) transport between the density surfaces (mean ± monthly s.d.) is labelled red (blue), with the net transport black. The arrows indicate the directions of diapycnal transformation. **b**, The overturning streamfunction with respect to temperature space, with a maximum reached at 3.7 °C. **c**, The overturning streamfunction with respect to salinity space, with a maximum reached at 34.90. Shaded grey area in **b** and **c** is monthly s.d.

Weak volume flux in density space

An accounting of the horizontal transport in each density layer (Fig. 1b) reveals the weak diapycnal mass flux. Even though large incoming and outgoing transports are observed in each layer, the net transports are quite small. For example, in the upper layer between 27.32 and $27.70\,\mathrm{kg\,m^{-3}}$, the transport of the incoming waters is $11.0\pm2.4\,\mathrm{Sv}$, of which $7.6\pm2.3\,\mathrm{Sv}$ exits the basin within the same density layer. The resultant net transport, $3.4\pm1.3\,\mathrm{Sv}$, contributes to the diapycnal mass flux by transforming to the LSW layer (assuming that all the diapycnal transformation occurs between neighbouring layers). In the LSW layer (27.70–27.80 kg m $^{-3}$), the net volume flux is $-3.9\pm1.9\,\mathrm{Sv}$, which indicates a net production of the LSW. As the transformation rate from the upper layer is 3.4 Sv, there must be a small transformation (~0.5 Sv) from the denser layer (that is, the NEADW layer) into the LSW layer. In the overflow water layers, net transports of 2.8 ± 1.0 and $-1.3\pm0.5\,\mathrm{Sv}$ were observed

in the NEADW layer (27.80–27.89 kg m⁻³) and in the DSOW layer (>27.89 kg m⁻³), respectively. Such a transport structure suggests a possible transformation from the NEADW to the DSOW within the Labrador Sea. As shown in Fig. 1a, there is, indeed, a small overturning cell present in these deep layers.

The weak diapycnal mass flux across OSNAP West is reflected by the small difference in the isopycnal (that is, density surfaces) slopes that bound the waters of the WGC and the LC. These comparable isopycnal slopes stand in stark contrast to the significant difference in the isotherm and isohaline slopes (Fig. 2a,b). This contrast indicates a strong density compensation by the temperature and salinity in the boundary current, which we explore next.

Strong volume flux in temperature-salinity space

To illustrate the impact of density compensation, we gridded the mean transports in potential temperature and salinity $(\theta$ –S) space

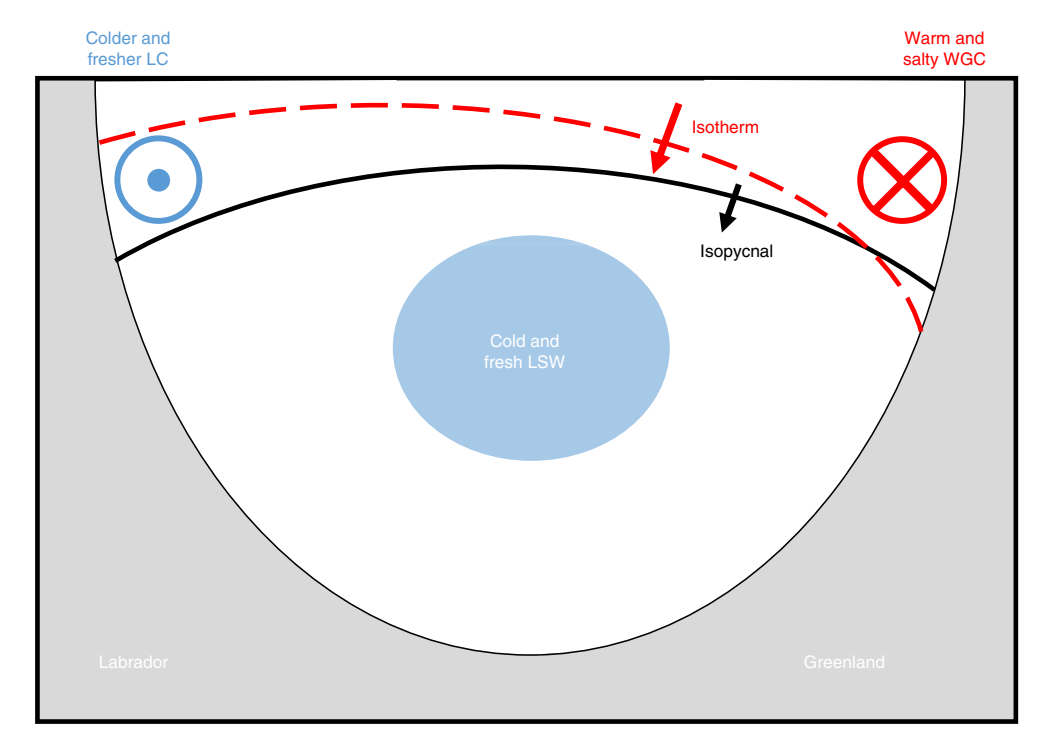


Fig. 4 | A schematic of the transformation along OSNAP West. Warm and salty waters enter the basin via the WGC and exit in the LC with cold and fresh anomalies, a result from the exchange between the boundary current and the cold and fresh basin interior. The resultant sharp tilt of isotherm from the WGC to the LC (red dashed line) suggests a strong transformation with respect to temperature space (red arrow). In contrast, the isopycnal slope is comparable on both sides of the basin due to density compensation, which results in a weak diapycnal transformation (black arrow).

(Fig. 3a). The transport in each θ -S grid represents the total volume flux across the OSNAP West section with shared temperature and salinity (Methods), and is therefore useful in diagnosing water-mass transformation in terms of the properties. In the upper layer, 9.5 ± 2.4 Sv of the warm and salty incoming waters (transport-weighted mean $\bar{\theta} \approx 4.7$ °C and $\bar{S} \approx 34.84$) become colder and fresher ($\bar{\theta} \approx 3.3$ °C, $\bar{S} \approx 34.67$) when exiting the basin. As these thermal and haline changes largely occur along isopycnals, most of these waters $(6.0 \pm 2.2 \,\text{Sy})$ are exported in the same density class. The property changes for the remaining 3.5 ± 1.3 Sv are not density compensated and, as such, are transformed to the LSW layer, as discussed above. Similar along-isopycnal transformation of temperature and salinity takes place in the other deep layers: in the LSW layer, the transformation is 12.4 ± 2.8 Sv with significant property changes (from $\bar{\theta} \approx 3.8$ °C, $\bar{S} \approx 34.92$ to $\bar{\theta} \approx 3.4$ °C, $\bar{S} \approx 34.87$), in the NEADW layer it is 6.0 ± 1.3 Sv with smaller property changes (from $\bar{\theta} \approx 2.9$ °C, $\bar{S} \approx 34.93$ to $\bar{\theta} \approx 2.8$ °C, $\bar{S} \approx 34.92$) and in the DSOW layer it is 1.1 ± 0.3 Sv (from $\bar{\theta} \approx 1.9$ °C, $\bar{S} \approx 34.91$ to $\bar{\theta} \approx 1.8$ °C, $\bar{S} \approx 34.90$).

Collectively, these analyses show that, although convection during the OSNAP observational period produced a large transformation of temperature and salinity, a weak diapycnal mass flux (and therefore a weak MOC) resulted because the thermal and haline changes in the boundary current primarily occurred along isopycnals. This finding emphasizes the important role of density compensation in setting the overturning strength in the Labrador Sea. If we consider transformation in temperature and salinity space separately, the resultant 'MOC' (by using the term MOC in temperature or salinity space, we mean the net transport across isotherms or isohalines) is as large as $13.9 \pm 3.0 \, \mathrm{Sv}$ in temperature space (MOC₆; Fig. 3b) and $11.4 \pm 2.8 \, \mathrm{Sv}$ in salinity space (MOC₆; Fig. 3c). Both of these estimates are 3-4 times greater than the MOC in density space. Many models are known to exhibit property biases in the Labrador Sea¹⁸, especially for salinity^{19,20} due to the large uncertainties in modelling the

hydrographic cycle, sea-ice interactions, Greenland ice-sheet melting and the freshwater pathways and/or mixing. Such salinity biases may lead to a temperature-dominated density structure across the basin, such that the transformation across isopycnals (that is, the MOC) would resemble the much stronger transformation across isotherms (that is, MOC_{θ}) (Fig. 4). It is also possible that salinity biases change the pattern of convection (by, for example, producing too much deep water and/or producing it in areas outside the observed region²¹) and/or influence the relative proportion of isopycnal and diapycnal mixing between the boundary current and the basin interior. We surmise that in both cases an overestimate of MOC may result, which has the effect of exaggerating the impact of convection²².

Although this 21-month record provides clear evidence for a density-compensated MOC in the Labrador Sea, the relatively short time series begs the question as to the representativeness of this time period. We examined this question by repeating our analysis with an ocean reanalysis dataset GloSea5 that represents well the observed water mass distribution and velocity structure across the Labrador Sea (Methods and Extended Data Figs. 1-3). The simulated MOC during August 2014 to April 2016 is 2.3 ± 1.2 Sv. The mean MOC over the 25-year domain of the reanalysis (1993–2017) is 2.7 Sv with a monthly s.d. of 2.1 Sv. Interestingly, during the strongest convective period (1993-1996), the MOC is as low as 2.0 Sv. All of these values are comparable to the OSNAP observations, as well as to estimates from hydrographic sections during the 1990s⁵. In addition, the large overturnings in temperature space $(13.3 \pm 5.6 \text{ Sy})$ and in salinity space $(17.6 \pm 4.7 \,\mathrm{Sy})$ from 1993 to 2017 show a consistent picture of strong along-isopycnal mixing between the boundary current and the basin interior. Thus, it is suggested that (1) the minimal contribution of the Labrador Sea convection to the total overturning in the subpolar gyre is probably representative of longer time periods and (2) density compensation of the large temperature and salinity changes is primarily responsible for the disconnect between convection and overturning in this basin.

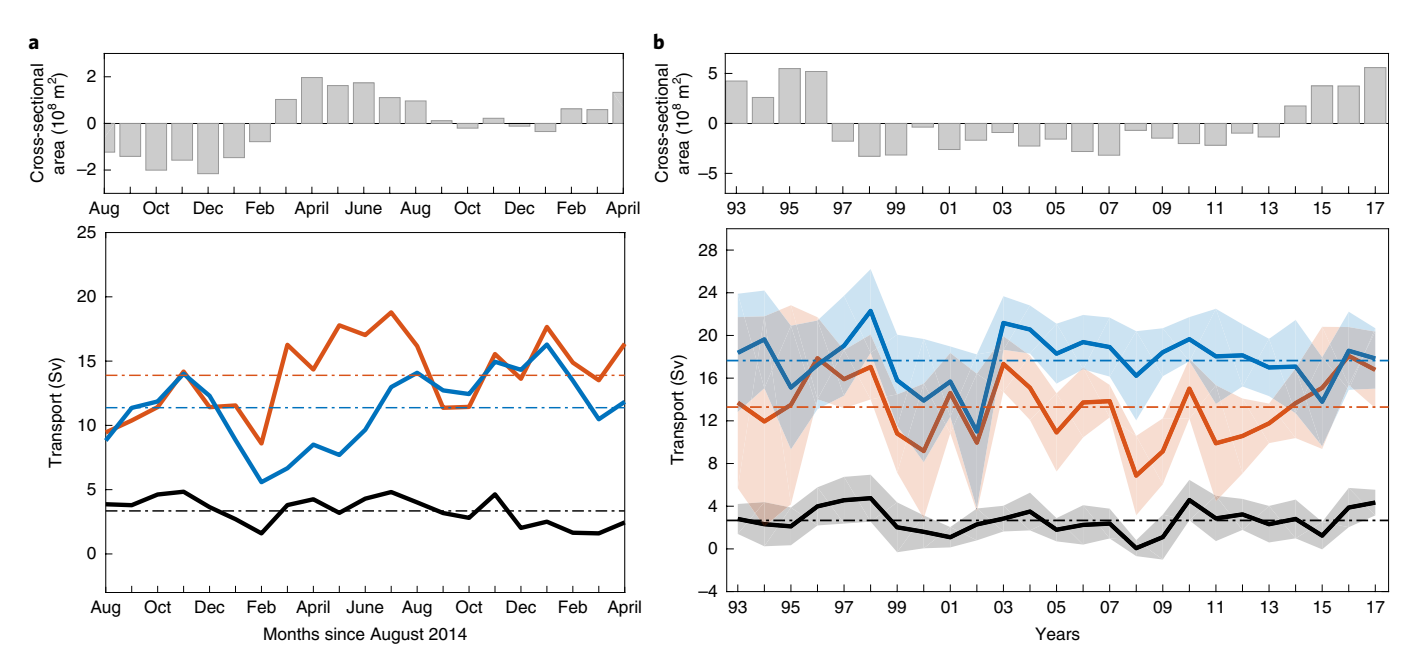


Fig. 5 | Variability of LSW volume and overturning transports. a, Observed monthly time series of newly formed LSW volume anomalies (relative to the 21-month mean; grey bars), MOC_{σ} (orange), MOC_{σ} (blue) and MOC (black) along OSNAP West. Coloured dashed lines indicate the 21-month mean of the overturning transports in each coordinate. **b**, Simulated annual time series of newly formed LSW volume (grey bars), MOC_{σ} (orange), MOC_{σ} (blue) and MOC (black) from GloSea5. Colour shading indicates the monthly s.d. for each year. All the time series are detrended. The results based on original (that is, non-detrended) time series yield similar conclusions.

Temporal variability of the overturning transports

We now turn our attention to the temporal variability of the overturning transports in the Labrador Sea. The observed monthly overturning transports are compared to the amount of newly formed LSW (that is, the product of convection) volume across OSNAP West (Fig. 5a). The volume is characterized as the cross-sectional area (m²) with a low potential vorticity (PV $\leq 6 \times 10^{-12} \,\mathrm{m}^{-1} \,\mathrm{s}^{-1}$) in Fig. 2c, the variability of which represents well the variability of the total newly formed LSW volume within the entire Labrador Sea (that is, the total volume of low PV in the basin; Extended Data Fig. 4). The maximum LSW volume occurred in April 2015, after which cold and fresh LSW was exported out of the basin via the LC. The cold and fresh anomalies in the LC enhanced the cross-sectional temperature and salinity difference and resulted in increases in MOC_{θ} and MOC_{s} . Although MOC_{θ} and MOC_{s} depend on differences in temperature and salinity across the basin, the temporal variability of MOC_{θ} correlates more with temperature anomalies in the outgoing LC, whereas MOC_s correlates more with the incoming salinity anomalies in the WGC (Extended Data Fig. 5).

Density compensation results in a weak monthly variability of the MOC, with no direct linkage to convection (Fig. 5a). We note that the observed variability of the diapycnal mass flux along OSNAP West does not reflect the variability of the total diapycnal transformation in the Labrador Sea (that is, northwest of OSNAP West) because the system is not in a steady state. The total diapycnal transformation exhibits a much stronger monthly variability in response to surface forcing and diapycnal mixing in the basin interior, and is mostly damped by volume changes in the isopycnal layers (Extended Data Fig. 6). In short, the LSW production variability does not translate to the MOC variability.

The observed monthly variability of the overturning transport is well simulated in GloSea5 (Extended Data Fig. 7). Compared to the monthly climatology over the 1993–2017 time period, simulated MOC and MOC $_{\rm s}$ during the OSNAP period (August 2014 to April 2016) do not stand out. MOC $_{\rm s}$, however, has a stronger and earlier peak (June compared to October for the long-term mean).

This difference is probably attributable to an enhanced convection during the OSNAP years, which can lead to colder anomalies exported to the boundary current at a faster rate⁴.

On interannual timescales, the volume of newly formed LSW correlates with MOC_a (r = 0.54), with the former leading by one year (Fig. 5b). As on monthly timescales in the observational record, the interannual variability of MOC_{θ} from this modelled time series is related to temperature anomalies in the LC (Extended Data Fig. 8), which are the product of the exchange with the interior. In contrast, no significant correlation is found between the LSW volume and MOC_s (r = -0.20). We explain this result by noting that changes in the salinity of the incoming WGC, the freshwater flux from the Arctic and the freshwater cycle can all impact salinity variability and thus MOC_s in the basin. Although temperature transformation seems tightly coupled to convective heat loss in the interior, the primary cause of the salinity transformation awaits further investigation. Finally, MOC remains low throughout the time series and shows insignificant correlation (r = 0.11) with the LSW volume variability. Such a weak correlation and the persistently low MOC magnitude in the Labrador Sea over the past two decades, which contain periods of both strong and intermediate convections, provide compelling evidence that density compensation explains the minimal imprint of the Labrador Sea convection on the MOC.

Discussions and implications

We present observational evidence for a significant density compensation of the mixing between the boundary current and the basin interior in the Labrador Sea, which serves to diminish the impact of convection on the MOC. This finding highlights the critical relationship between temperature and salinity in setting the density structure, thereby the MOC, in the basin. Although global warming and emerging freshwater accumulation from Greenland^{23,24} may lead to a weakened convection in the Labrador Sea, it remains unclear whether these changes would break the compensated influence of temperature and salinity on density, and thereby modify the MOC. As such, this work suggests that models need to correctly simulate

the salinity (as well as temperature) field to adequately reproduce the MOC and predict its response to future climate change.

Finally, we note that Lozier et al. 10 offered a reconciliation between the recent OSNAP results and past studies 3,25 that have used mid-depth densities in the Labrador Sea as proxies for the downstream MOC strength. Specifically, they note that a reconciliation "... is possible if the density anomalies in the Labrador Sea are signatures of upstream density anomalies imported from the eastern subpolar gyre and/or have a remote impact on the overturning between Greenland and Scotland". Our work here suggests that the temperature and salinity anomalies formed via convection might also serve as proxies for the same reason, but they are unlikely drivers of the downstream MOC variability. Indeed, a recent estimate of the mean MOC in the subpolar North Atlantic, reconstructed from combined shipboard current measurements and hydrographic profiles, suggests that the Nordic Seas, rather than the Labrador Sea, are "key to the state of the MOC" 26.

Online content

Any methods, additional references, Nature Research reporting summaries, source data, extended data, supplementary information, acknowledgements, peer review information; details of author contributions and competing interests; and statements of data and code availability are available at https://doi.org/10.1038/s41561-019-0517-1.

Received: 13 June 2019; Accepted: 26 November 2019; Published online: 13 January 2020

References

- Wood, R. A., Keen, A. B., Mitchell, J. F. & Gregory, J. M. Changing spatial structure of the thermohaline circulation in response to atmospheric CO₂ forcing in a climate model. *Nature* 399, 572–575 (1999).
- Rahmstorf, S. et al. Exceptional twentieth-century slowdown in Atlantic Ocean overturning circulation. Nat. Clim. Change 5, 475–480 (2015).
- Thornalley, D. J. et al. Anomalously weak Labrador Sea convection and Atlantic overturning during the past 150 years. Nature 556, 227–230 (2018).
- 4. Straneo, F. On the connection between dense water formation, overturning, and poleward heat transport in a convective basin. *J. Phys. Oceanogr.* **36**, 1822–1840 (2006).
- Pickart, R. S. & Spall, M. A. Impact of Labrador Sea convection on the North Atlantic meridional overturning circulation. *J. Phys. Oceanogr.* 37, 2207–2227 (2007).
- Rhein, M. et al. Labrador Sea water: pathways, CFC inventory, and formation rates. J. Phys. Oceanogr. 32, 648–665 (2002).
- Marsh, R. Recent variability of the North Atlantic thermohaline circulation inferred from surface heat and freshwater fluxes. J. Clim. 13, 3239–3260 (2000).

- 8. Talley, L. D. Shallow, intermediate, and deep overturning components of the global heat budget. *J. Phys. Oceanogr.* **33**, 530–560 (2003).
- Xu, X., Rhines, P. B. & Chassignet, E. P. On mapping the diapycnal water mass transformation of the upper North Atlantic Ocean. J. Phys. Oceanogr. 48, 2233–2258 (2018).
- Lozier, M. S. et al. A sea change in our view of overturning in the subpolar North Atlantic. Science 363, 516–521 (2019).
- Lozier, M. S. et al. Overturning in the Subpolar North Atlantic Program: a new international ocean observing system. *Bull. Am. Meterol. Soc.* 98, 737–752 (2017).
- Yashayaev, I. & Loder, J. W. Further intensification of deep convection in the Labrador Sea in 2016. Geophys. Res. Lett. 44, 1429–1438 (2017).
- Lavender, K. L., Davis, R. E. & Owens, W. B. Mid-depth recirculation observed in the interior Labrador and Irminger Seas by direct velocity measurements. *Nature* 407, 66–69 (2000).
- Cuny, J., Rhines, P. B., Niiler, P. P. & Bacon, S. Labrador Sea boundary currents and the fate of the Irminger Sea water. J. Phys. Oceanogr. 32, 627–647 (2002).
- Spall, M. A. Boundary currents and watermass transformation in marginal seas. J. Phys. Oceanogr. 34, 1197–1213 (2004).
- Katsman, C. A., Spall, M. A. & Pickart, R. S. Boundary current eddies and their role in the restratification of the Labrador Sea. J. Phys. Oceanogr. 34, 1967–1983 (2004).
- Curry, B., Lee, C. M. & Petrie, B. Volume, freshwater, and heat fluxes through Davis Strait, 2004–05. J. Phys. Oceanogr. 41, 429–436 (2011).
- Menary, M. B. et al. Exploring the impact of CMIP5 model biases on the simulation of North Atlantic decadal variability. *Geophys. Res. Lett.* 42, 5926–5934 (2015).
- Schneider, B., Latif, M. & Schmittner, A. Evaluation of different methods to assess model projections of the future evolution of the Atlantic meridional overturning circulation. *J. Clim.* 20, 2121–2132 (2007).
- Zhang, X. et al. Detection of human influence on twentieth-century precipitation trends. Nature 448, 461–465 (2007).
- Heuzé, C. North Atlantic deep water formation and AMOC in CMIP5 models. Ocean Sci. 13, 609–622 (2017).
- Li, F. et al. Local and downstream relationships between Labrador Sea water volume and North Atlantic meridional overturning circulation variability. *I. Clim.* 32, 3883–3898 (2019).
- 23. IPCC Climate Change 2013: The Physical Science Basis (eds Stocker, T. F. et al.) (Cambridge Univ. Press, 2013).
- Böning, C. W., Behrens, E., Biastoch, A., Getzlaff, K. & Bamber, J. L. Emerging impact of Greenland meltwater on deepwater formation in the North Atlantic Ocean. *Nat. Geosci.* 9, 523–527 (2016).
- Jackson, L. C., Peterson, K. A., Roberts, C. D. & Wood, R. A. Recent slowing of Atlantic overturning circulation as a recovery from earlier strengthening. *Nat. Geosci.* 9, 518–522 (2016).
- Chafik, L. & Rossby, T. Volume, heat, and freshwater divergences in the subpolar North Atlantic suggest the Nordic seas as key to the state of the meridional overturning circulation. *Geophys. Res. Lett.* 46, 4799–4808 (2019).

Publisher's note Springer Nature remains neutral with regard to jurisdictional claims in published maps and institutional affiliations.

© The Author(s), under exclusive licence to Springer Nature Limited 2020

Methods

Observational data across the OSNAP array. We used gridded property and velocity data across the OSNAP West section for each 30-day period between August 2014 and April 2016. The grid, following the section, has a variable horizontal resolution with an upper limit of ~25 km, and a uniform vertical resolution of 20 m. These gridded data are primarily based on continuous temperature, salinity and velocity measurements from 20 high-resolution moorings (~15 km apart) deployed in both boundaries of the Labrador Sea since August 2014 (Fig. 1b gives the location). The gridded data also incorporate many other observations in the region, which include those from Argo, satellite altimetry and shipboard conductivity, temperature and depth stations.

In the boundaries covered by the moorings, moored property and velocity measurements were interpolated onto the predefined grid mentioned above. Away from the moorings in the basin interior, the geostrophic velocities were calculated from the two bounding dynamic height moorings by referencing to the time-mean surface velocities provided by satellite altimetry. In addition, a spatially uniform compensation velocity was added at each 30-day period to yield a 1.6 Sv southward net transport across the section to match the long-term observations across the Davis Strait¹⁷. Property fields in the basin interior down to 2,000 m were constructed via an objective analysis method ^{10,27,28}. The objective analysis method used temperature and salinity from Argo profiles, OSNAP moorings and World Ocean Atlas 2013 (WOA13) climatology. There were, on average, 99 Argo profiles in the Labrador Sea each month between 2014 and 2016. Below 2,000 m, data from the hydrographic sections during the summers of 2014 and 2016 were used.

Lozier et al. 10 gives a detailed description on the calculation method and the data products from OSNAP.

Reanalysis GloSea5. We also used data from the global ocean and sea-ice reanalysis GloSea5^{25,29}, which uses the NEMO GO5 model with a nominal resolution of 0.25° and 75 vertical layers³⁰ and the NEMOVAR v13 assimilation scheme³¹. The assimilated observations were: in-situ and satellite sea-surface temperatures, subsurface ocean profiles of temperature and salinity, sea-ice concentration and sea-level anomalies. The experiment is described in more detail in Jackson et al.²⁵.

To show that the reanalysis data can adequately simulate the property field in the Labrador Sea, we compared the cross-sectional potential vorticity, temperature, salinity, density and velocity fields between GloSea5 and the OSNAP data during the observational period (Extended Data Figs. 1–3). Overall, the magnitude and variability of MOC in the reanalysis compares fairly well with the observations.

There are two differences to note. First, the salinity gradient between the LC and the WGC is stronger in the reanalysis. Second, the maximum overturning in the reanalysis takes place at a denser level ($\sim\!27.80\,kg\,m^{-3};$ Extended Data Fig. 3a) compared to the observations ($\sim\!27.70\,kg\,m^{-3};$ Fig. 1a), a difference that is possibly attributable to a weaker stratification in the deep Labrador Sea in GloSea5.

Water mass definition in density space. Deep water masses in the Labrador Sea can be identified from property fields ¹². Along OSNAP West, LSW is identified by a low salinity, relatively low temperature, low potential vorticity (Fig. 2) and low potential density (σ_{0} , referenced to the surface), which is generally between 27.70 and 27.80 kg m⁻³. Below LSW, the NEADW, with a low temperature and high salinity, occupies the layer between 27.80 and 27.89 kg m⁻³. Finally, the layer below 27.89 kg m⁻³ contains the DSOW, which has the lowest temperature and a relatively low salinity. The water mass distribution shown here is very similar to those discussed in Yashayaev and Loder ¹².

In this study, the water masses are defined only by σ_{θ} specified above because of its direct relationship with the stratification and potential energy. In addition, a definition in neutral density space does not show qualitative difference from that in σ , space

Calculation of overturning in longitude–density space. In this study, the MOC is calculated as the maximum of the overturning streamfunction in σ_{θ} space:

$$\begin{aligned} & \text{MOC}(t) = \text{max} \Psi(\sigma_{\theta}, t) \\ &= \text{max} [-\int_{\sigma_{\theta_{\text{max}}}}^{\sigma_{\theta}} \int_{x_{\epsilon}}^{x_{w}} \nu(x, \sigma_{\theta}, t) \mathrm{d}x \mathrm{d}\sigma_{\theta}] \end{aligned} \tag{1}$$

where $v(x,\sigma_{\theta},t)$ represents the transport component per unit length per unit density $((\text{m}^3\,\text{s}^{-1})\text{m}^{-1}(\text{kg}\,\text{m}^{-3})^{-1})$ that is perpendicular to the section. A positive v indicates a flux into the basin (that is, northwestward across OSNAP west). x_w denotes the westernmost position of the section, which is the Labrador Coast, and x_c denotes the easternmost position, which is the southwestern tip of Greenland. The overturning streamfunction $\Psi(\sigma_{\theta},t)$ is integrated from high density $(\sigma_{\theta \max})$ to low density (σ_{θ}) , which is different from the traditional calculation (from low density to high density). The latter method inevitably includes the southward flux of the lightest waters along the Labrador shelf that are not involved in the diapycnal transformation in the basin, which leads to a smaller estimation of MOC (Extended Data Fig. 9). Finally, we note that, in the Labrador Sea, the strength of the MOC in neutral density space is nearly identical to that in σ_{θ} space σ_{θ} .

In Fig. 1a, the 21-month mean $\overline{\Psi(\sigma_{\theta},t)}$ is shown, whose maximum is 2.5 Sv, reached at $27.70\,\mathrm{kg}\,\mathrm{m}^{-3}$. This maximum is smaller than the mean of the monthly

maximum streamfunctions, that is, $\overline{\max \Psi(\sigma_{\theta}, t)}$, which is 3.3 Sv. This is because when averaging monthly streamfunctions, the level at which the maximum is reached is not taken into account ¹⁰. As such, the mean streamfunction results in a weaker overturning.

Calculation of overturning in θ -S **space.** To compute overturning in the θ -S space, we followed the approach in previous studies^{32,33} by first computing volume transport in θ -S space:

$$v^*(\theta^*, S^*, t) = \frac{1}{\Delta\theta\Delta S} \iint \delta_{\Delta\theta} \delta_{\Delta S} v(x, z, t) dx dz$$
 (2)

where $\delta_{\Delta\theta}$ and $\delta_{\Delta S}$ are defined as discrete delta functions, such that:

$$\delta_{\Delta\theta} = \begin{cases} 1, |\theta - \theta^*| \le \Delta\theta/2 \\ 0, & \text{elsewhere} \end{cases}$$
 (3)

$$\delta_{\Delta S} = \begin{cases} 1, |S - S^*| \leq \Delta S/2 \\ 0, \text{ elsewhere} \end{cases} \tag{4}$$

v(x,z,t) represents the velocity component that is perpendicular to the section (m s⁻¹), where x denotes the position between the Labrador Coast and Greenland and z denotes depth. As such, $v^*(\theta^*,S^*,t)$ is the transport over the bin area $\Delta\theta\times\Delta S$ at (θ^*,S^*) (units m³ s⁻¹°C⁻¹). After a series of sensitivity tests to assess which $\Delta\theta\times\Delta S$ best describes the temperature/salinity structure in the Labrador Sea, $\Delta\theta$ was prescribed as 0.1 °C and ΔS as 0.002. The overturning streamfunctions with respect to temperature, $\Psi_{\theta}(\theta,t)$, and salinity space, $\Psi_{S}(S,t)$, can then be obtained by integrating $v^*(\theta^*,S^*,t)$ along isotherms and isohalines according to:

$$\Psi_{\theta}(\theta, t) = \int_{\theta_{max}}^{\theta} \int_{S_{min}}^{S_{max}} v^{*}(\theta^{*}, S^{*}, t) dS^{*} d\theta^{*}$$
(5)

$$\Psi_{S}(S,t) = \int_{-S}^{S} \int_{\theta_{max}}^{\theta_{max}} v^{*}(\theta^{*}, S^{*}, t) d\theta^{*} dS^{*}$$

$$\tag{6}$$

Here $\Psi_{\vartheta}(\theta,t)$ and $\Psi_s(S,t)$ are both integrated from high to low values. Note that due to the high salinity contained in the NEADW layer, the salinity profile across OSNAP West is not monotonic with depth, different from the density and temperature. As such, the strength of Ψ_s can be influenced by the transport in the salty NEADW layer. To exclude this influence and to keep the calculation consistent with that in temperature space, we calculated Ψ_s only with waters lighter than 27.80 kg m⁻³. A test calculation of Ψ_s with all waters does not change any of our conclusions, but only results in a stronger Ψ_s .

Data availability

OSNAP data were collected and made freely available by the OSNAP project and all the national programs that contribute to it (https://www.o-snap.org/). Data from the full OSNAP array for the first 21 months (31 July 2014 to 20 April 2016) were used to produce the 30-day mean time series across the whole section, as well as the gridded property fields. This derived data is at http://doi.org/10.7924/r4z60gf0f. Data from GloSea5 (re-gridded to 1×1°) is available from http://marine.copernicus.eu/services-portfolio/access-to-products/ under product name GLOBAL_REANALYSIS_PHY_001_026. EN4.2.1 data used in Extended Data Figs. 4 and 6 were downloaded from https://www.metoffice.gov.uk/hadobs/en4/.

Code availability

The code used to generate MOC and transport in the temperature and salinity space can be accessed upon request to S.Z.

References

- Li, F., Lozier, M. S. & Johns, W. E. Calculating the meridional volume, heat, and freshwater transports from an observing system in the subpolar North Atlantic: observing system simulation experiment. *J. Atmos. Ocean. Technol.* 34, 1483–1500 (2017).
- Li, F. & Lozier, M. S. On the linkage between Labrador Sea water volume and overturning circulation in the Labrador Sea: a case study on proxies. *J. Clim.* 31, 5225–5241 (2018).
- Blockley, E. W. et al. Recent development of the Met Office operational ocean forecasting system: an overview and assessment of the new Global FOAM forecasts. Geosci. Model Dev. 7, 2613–2638 (2014).
- Megann, A. P. et al. GO 5.0: The joint NERC–Met Office NEMO global ocean model for use in coupled and forced applications. *Geotech. Model Dev.* 7, 1069–1092 (2014).
- Waters, J. et al. Implementing a variational data assimilation system in an operational 1/4 degree global ocean model. Q. J. R. Meteorol. Soc. 141, 333–349 (2015).
- 32. Zika, J. D., England, M. H. & Sijp, W. P. The ocean circulation in thermohaline coordinates. *J. Phys. Oceanogr.* **42**, 708–724 (2012).

 Xu, X., Rhines, P. B. & Chassignet, E. P. Temperature–salinity structure of the North Atlantic circulation and associated heat and freshwater transports. J. Clim. 29, 7723–7742 (2016).

Acknowledgements

S.Z., M.S.L. and F.L. gratefully acknowledge the Physical Oceanography Program of the US National Science Foundation (fund code 3331843). R.A. acknowledges support from NSF award OCE 1553593. L.J. is funded by the Copernicus Marine Environment Monitoring Service (CMEMS: 23-GLO-RAN). The authors acknowledge the work of K. A. Peterson in creating the GloSea5 reanalysis.

Author contributions

S.Z., M.S.L. and F.L. led the data analysis. F.L. conducted the MOC calculation. R.A. proposed and formulated the calculation for overturning in temperature and salinity

space. L.J. provided the GloSea5 data and assisted with the calculation of MOC. All the authors contributed to interpretation of the results and writing of the manuscript .

Competing interests

The authors declare no competing interests.

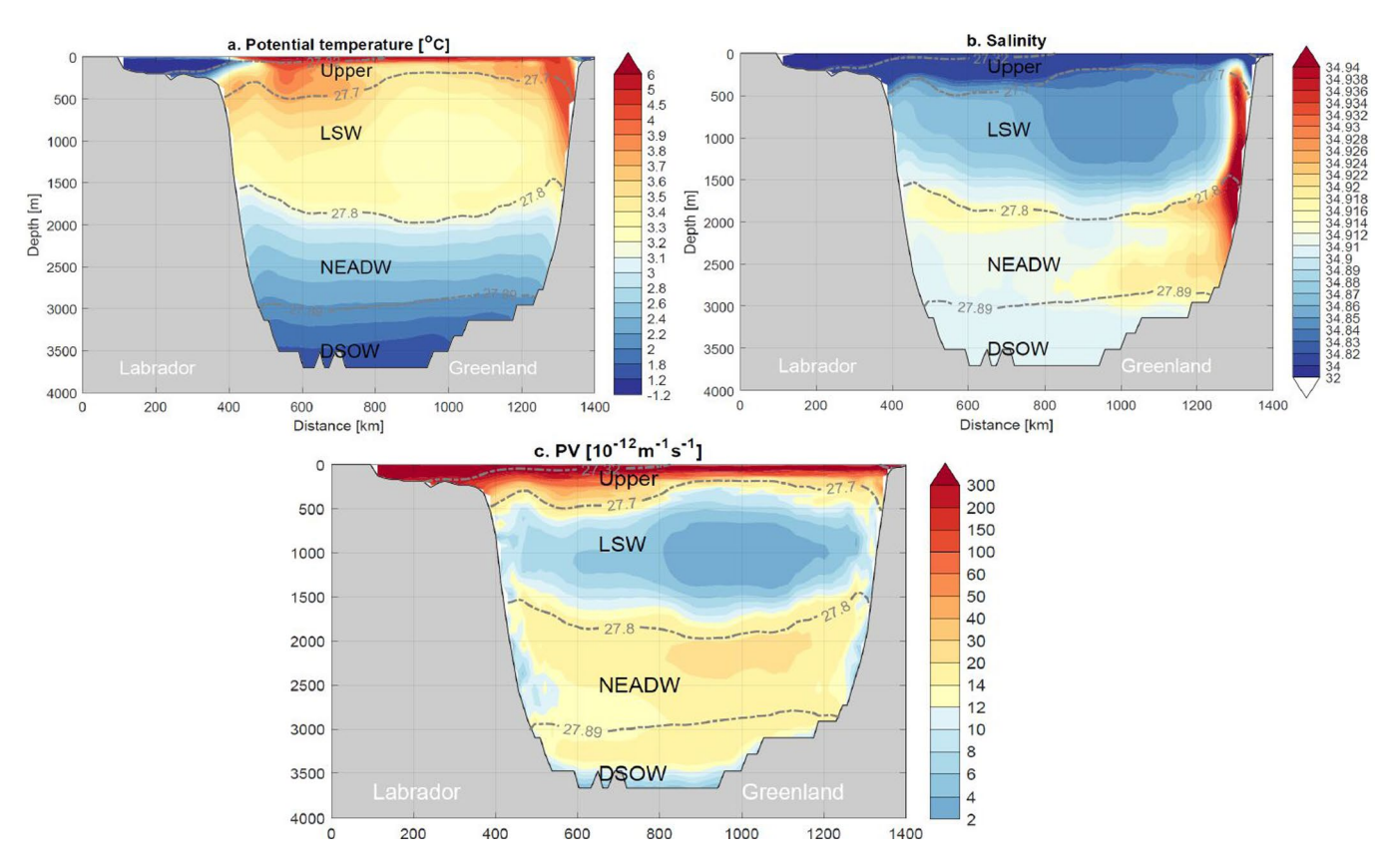
Additional information

Extended data is available for this paper at https://doi.org/10.1038/s41561-019-0517-1. **Supplementary information** is available for this paper at https://doi.org/10.1038/s41561-019-0517-1.

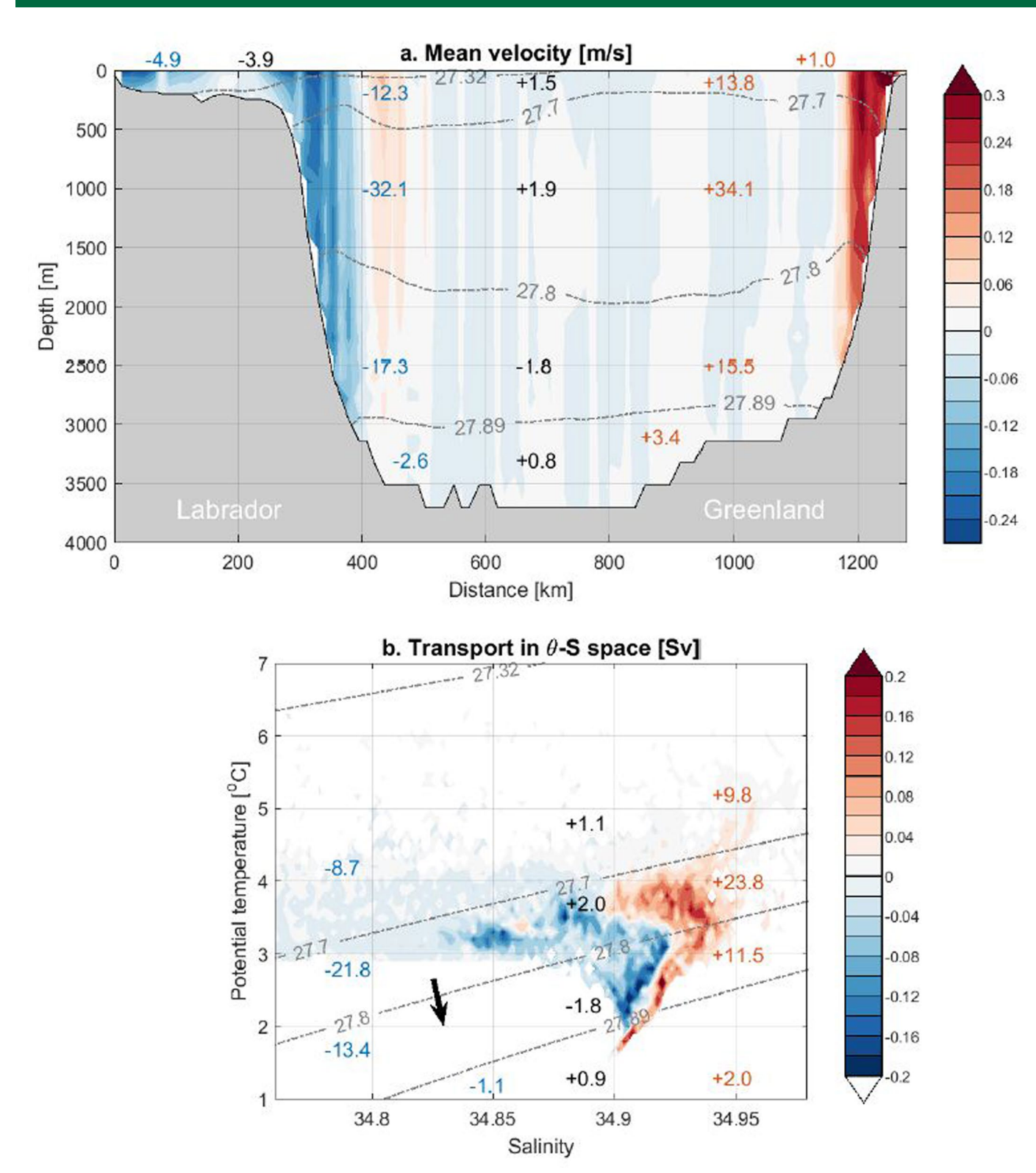
Correspondence and requests for materials should be addressed to S.Z.

Peer review information Primary Handling Editor: Heike Langenberg.

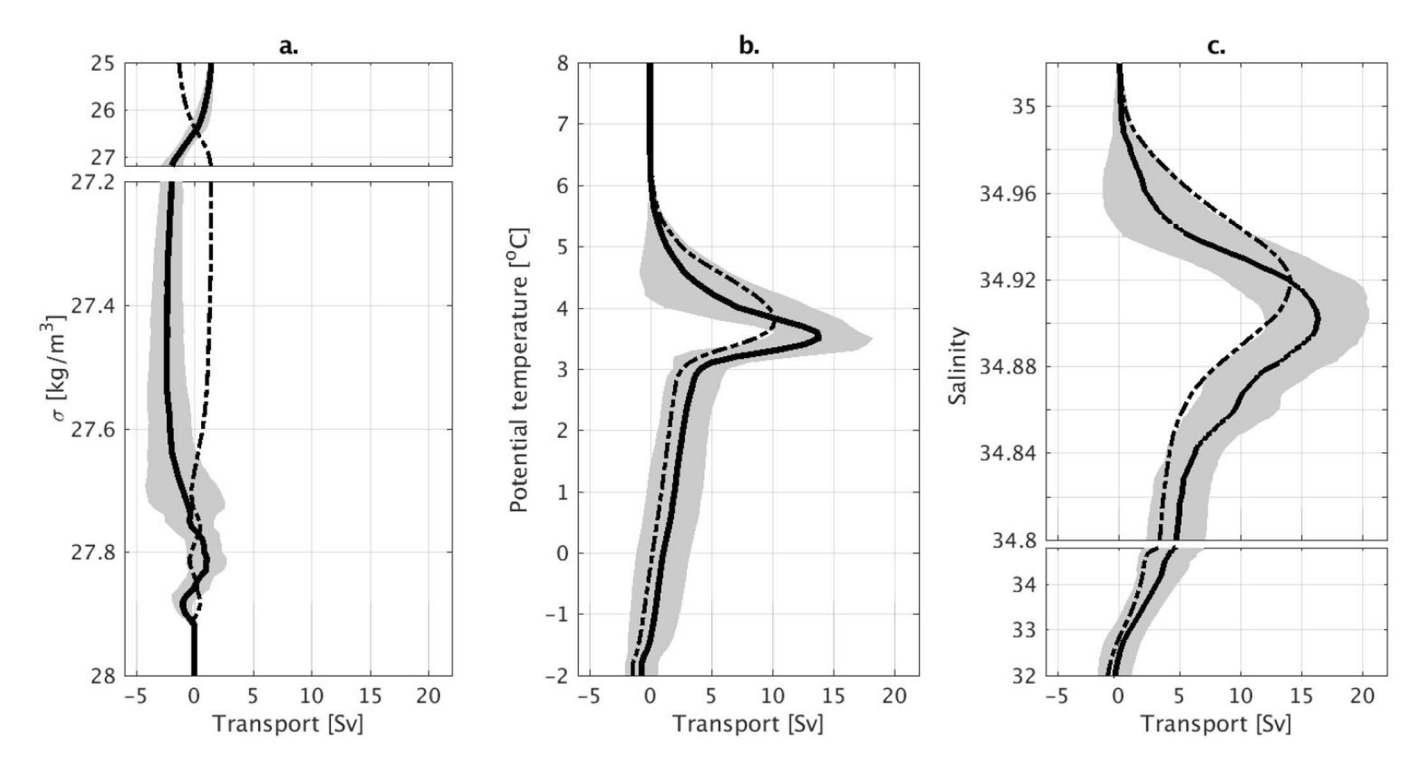
Reprints and permissions information is available at www.nature.com/reprints.



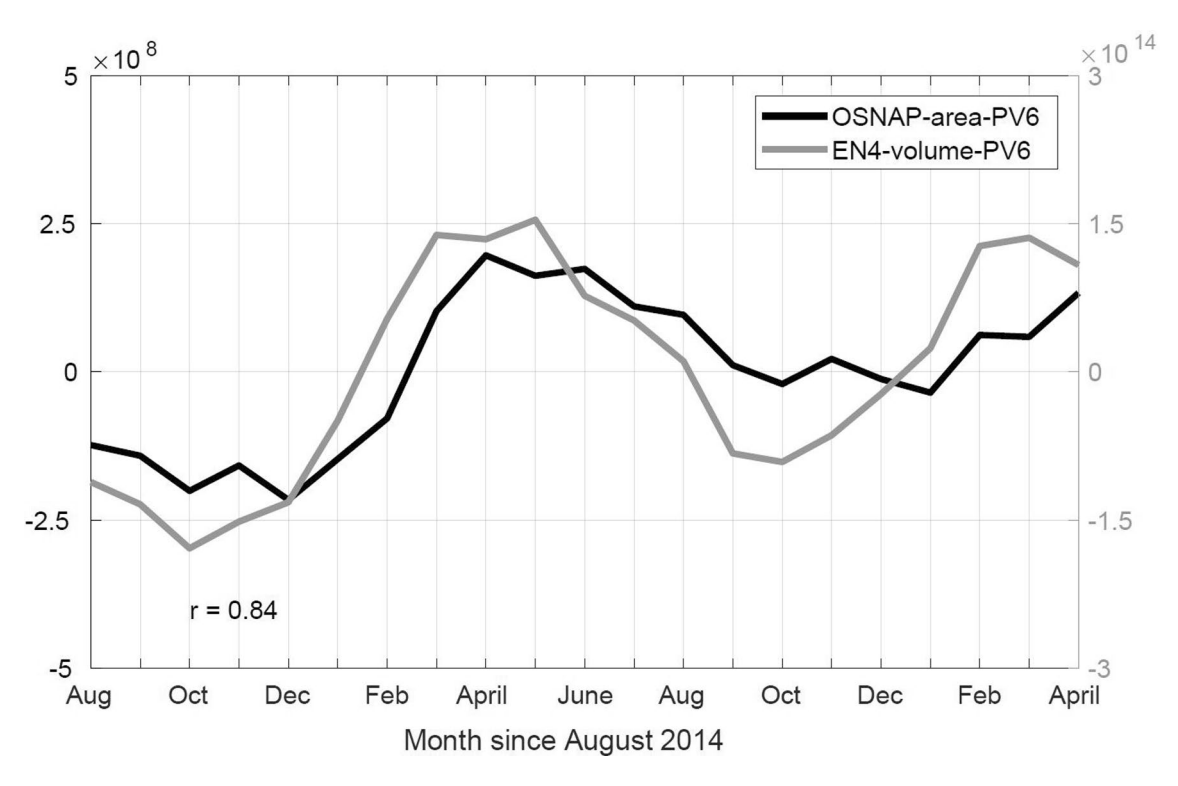
Extended Data Fig. 1 | Simulated mean property distribution in GloSea5. (a) Mean potential temperature averaged between August 2014 and April 2016 along simulated OSNAP West section. (**b**) Mean salinity from the same source. (**c**) Mean PV ($\times 10^{-12} m^{-1} s^{-1}$) from the same source. The simulated OSNAP West section is created using model grid points that minimize the distance from the grid locations to the observational locations. Temperature, salinity and PV are then extracted along the section. Note that the section definition allows for an accurate calculation of the transport on the model grid.



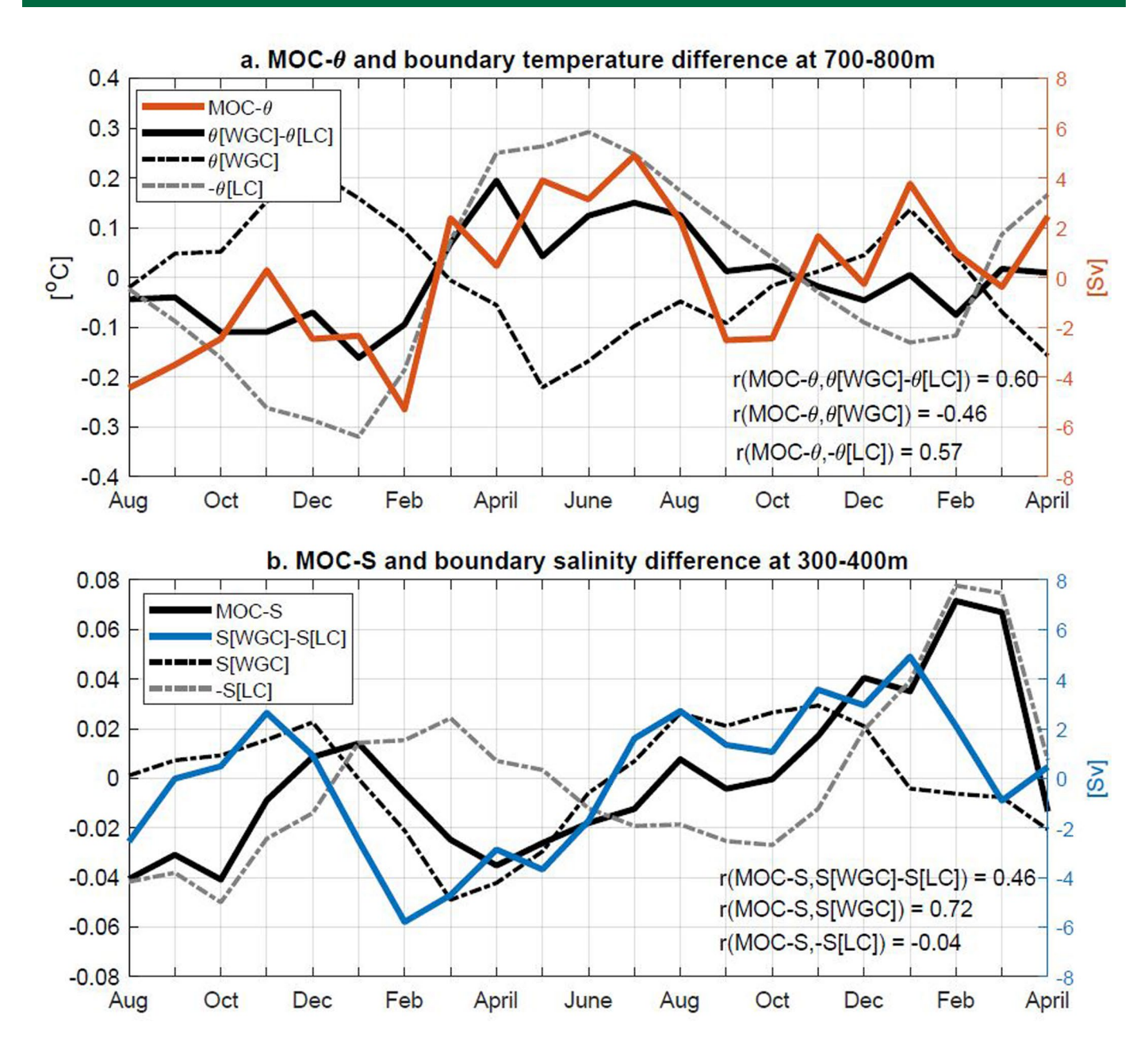
Extended Data Fig. 2 | Simulated mean circulation in GloSea5. (a) The mean velocity perpendicular to the simulated OSNAP West section during August 2014 and April 2016. Positive (negative) velocities indicate flow into (out of) the basin. Mean volume flux in each density class is labeled, similar to that in Fig. 1b. Note that the along-isopycnal transport in each layer is stronger in GloSea5 compared to the observations (Fig. 1b). This is because that when integrating the total positive/negative transport across the section, the recirculation branches in the basin interior are also included. (b) Mean volume flux in θ -S space from the reanalysis. Black arrow indicates direction of the diapycnal transformation.



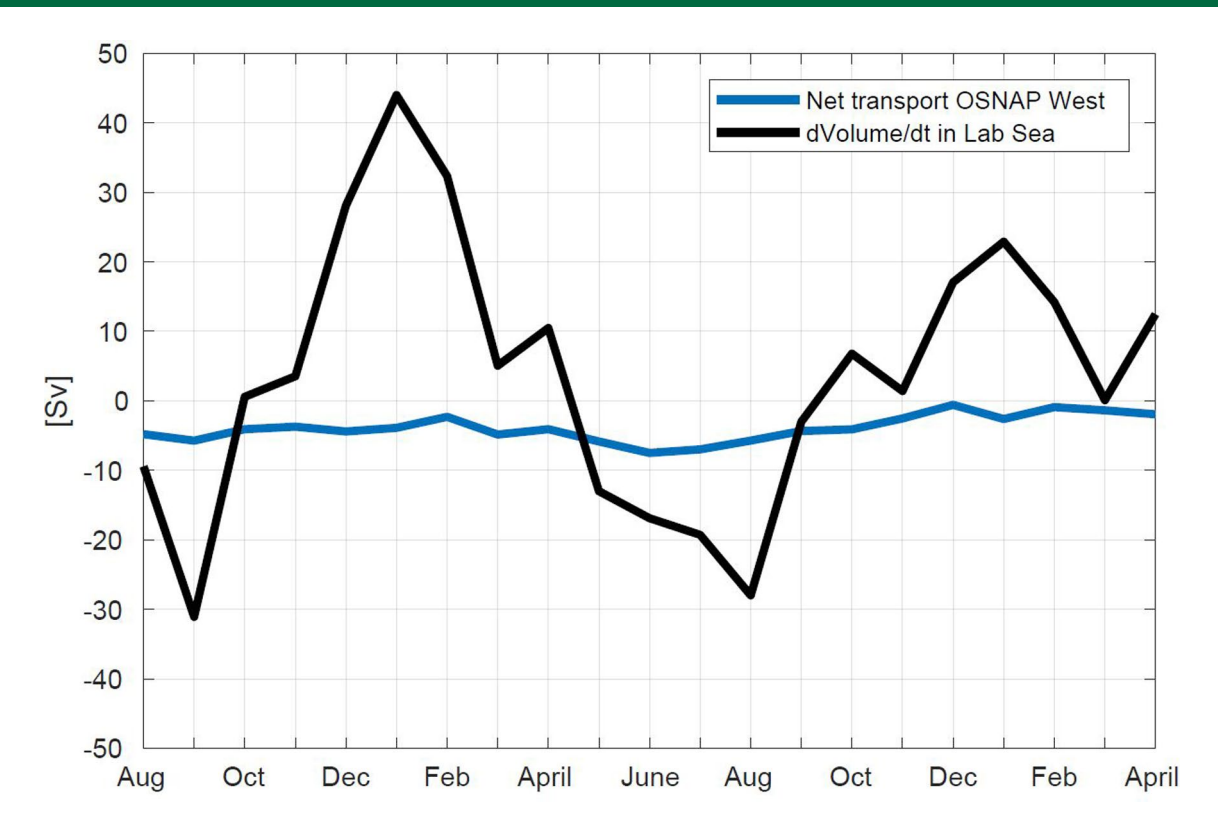
Extended Data Fig. 3 | Simulated mean overturning streamfunction in GloSea5. (a) The mean overturning streamfunction in density space during August 2014 - April 2016 (solid black), with monthly SD shaded in gray. Dashed curve indicates the overturning streamfunction averaged over the entire temporal domain from the reanalysis (that is 1993-2017). **(b)** Similar to (a), but in θ space. (c) Similar to (a), but in S space.



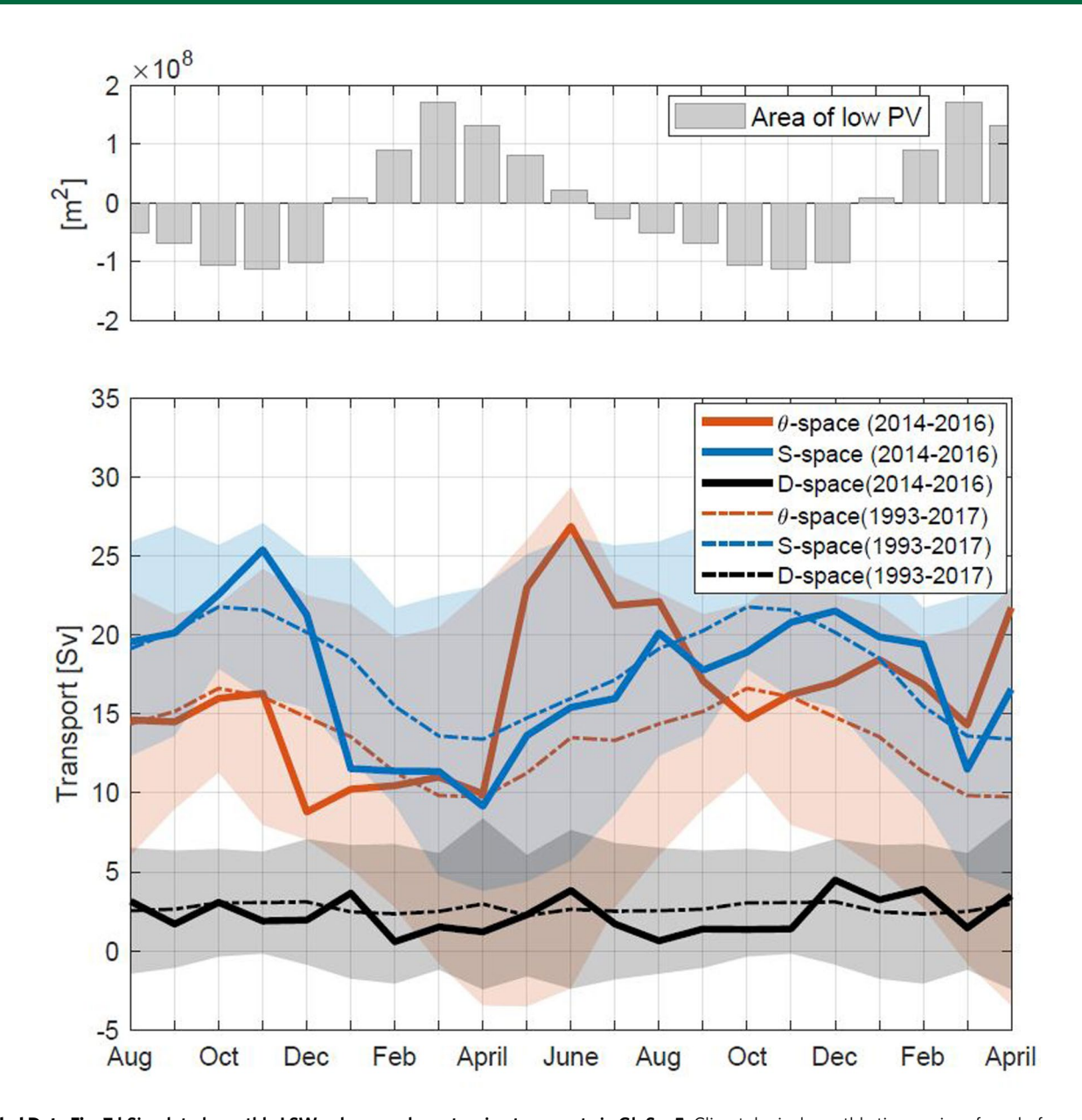
Extended Data Fig. 4 | **Observed monthly variability of LSW volume.** Monthly time series of the total area (unit: m^2) with low potential vorticity $(PV \le 6 \times 10^{-12} m^{-1} \text{s}^{-1})$ across OSNAP West from observations (black), and the total volume (unit: m^2) with low PV in the entire Labrador Basin (gray) from the Met Office Hadley Centre observational datasets EN4.2.1 (S. A. Good, M. J. Martin, M. J. & N. A. Rayner, N. A., *J. Geophys. Res. Oceans* **118**, 6704–6716; 2013). Plotted are the anomalies relative to the 21-month mean.



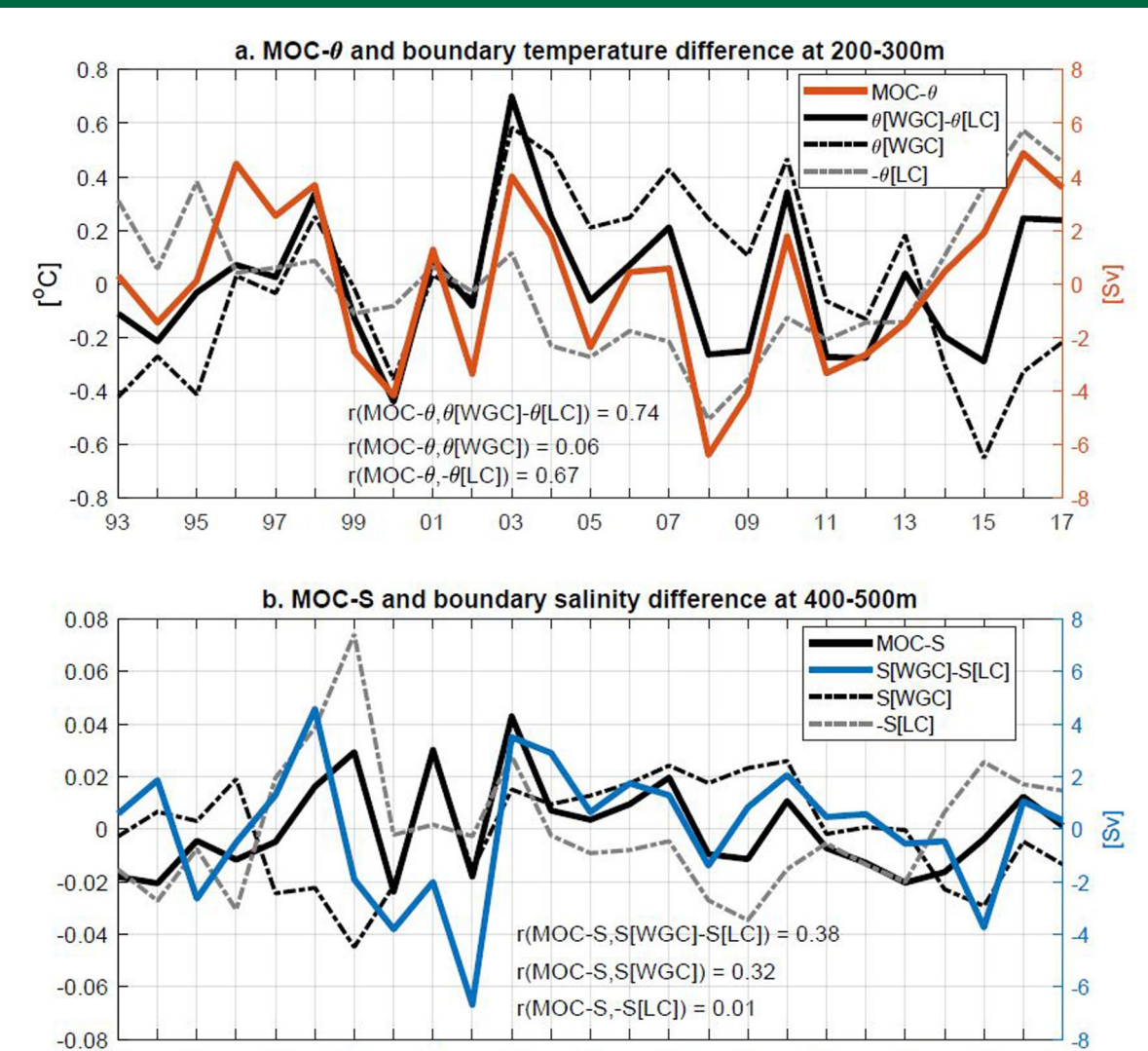
Extended Data Fig. 5 | Observed relationship between MOC_{θ} **(MOC_s) and temperature (salinity) distribution.** (a) Observed monthly anomalies of MOC_{θ} (orange) since August 2014 and potential temperature difference between the WGC and the LC (that is $\theta[WGC]-\theta[LC]$) at 700-800 m (solid black), the depths at which the correlation between the two time series is the strongest. The temperature anomalies for the WGC (that is $\theta[WGC]$) are plotted in dashed black and the negative temperature anomalies for the LC (that is $-\theta[LC]$) are shown in dashed gray. (b) Similar to (a), but for MOC_S and salinity anomalies in the boundary current.



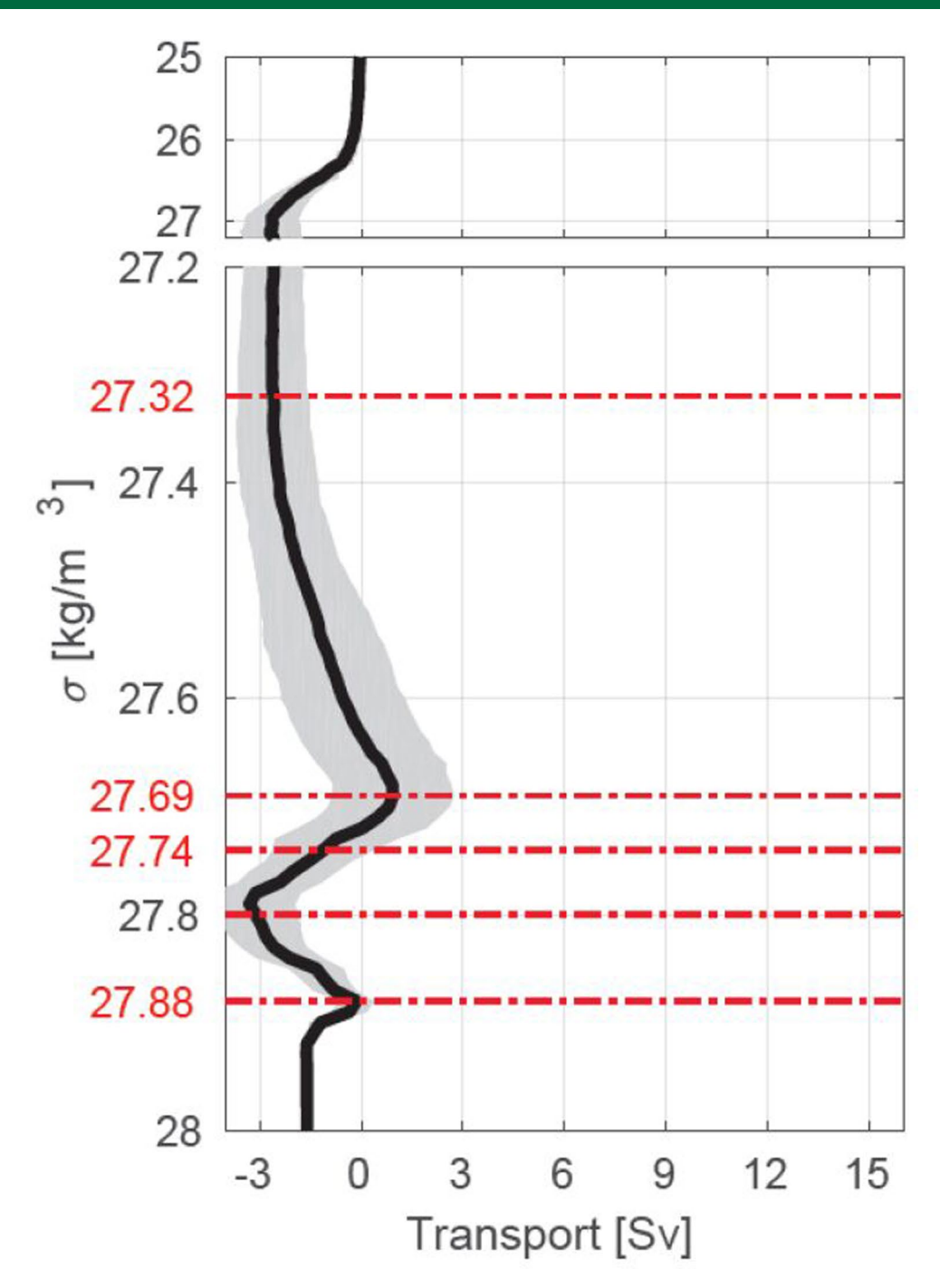
Extended Data Fig. 6 | Strong monthly LSW layer volume variability. Plotted in black is the LSW layer $(27.70-27.80 \, kg/m^3)$ volume variability within the Labrador Sea (northwest of OSNAP West) since August 2014, which is derived from EN4.2.1 (S. A. Good, M. J. Martin, M. J. & N. A. Rayner, N. A., *J. Geophys. Res. Oceans* **118**, 6704–6716; 2013). Observed monthly transport in the LSW layer across OSNAP West is plotted in blue. The variability between the two time series is similar (r = 0.61), but the magnitude differs significantly.



Extended Data Fig. 7 | Simulated monthly LSW volume and overturning transports in GloSea5. Climatological monthly time series of newly-formed LSW volume (gray bars), MOC_{σ} (dashed orange), MOC_{σ} (dashed blue), and MOC_{σ} (dashed black) from GloSea5 during 1993-2017. Shaded areas represent 2xstandard deviation of the annually varying transport for each month. The simulated transport time series during the OSNAP time period (August 2014 - April 2016) are plotted in solid colored lines.



Extended Data Fig. 8 | Relationship between interannual MOC_{θ} (MOC_{θ}) and temperature (salinity) distribution in GloSea5. (a) Simulated annual anomalies of MOC_{θ} (orange) and the temperature difference between the WGC and the LC (that is $\theta[WGC] - \theta[LC]$) at 200-300m (solid black). The depths between 200-300m are where the maximum correlation between MOC_{θ} and temperature difference is reached. The temperature anomalies for the WGC alone (that is $\theta[WGC]$) are plotted in dashed black and the minus temperature anomalies for the LC (that is $-\theta[LC]$) are plotted in dashed gray. (b) Similar to (a), but for MOC_{θ} and salinity anomalies in the boundary current.



Extended Data Fig. 9 | Observed overturning streamfunction with the traditional calculation. The 21-month mean overturning streamfunction integrated from low density to high density (solid black), with monthly standard deviation shaded in gray. The MOC with this calculation is $1.4 \pm 1.75v$ (see Methods).